

Supporting Information

Fabrication of Designable and Suspended Micro -fibers via Low-Voltage 3D

Micropatterning

Elisabeth L. Gill†‡, Samuel Willis†, Magda Gerigk†‡, Paul Cohen†, Duo Zhang†‡, Xia Li†
and Yan Yan Shery Huang†‡*

† Department of Engineering, University of Cambridge, Trumpington Street, Cambridge,
CB2 1PZ, UK

‡The Nanoscience Centre, University of Cambridge, 11 JJ Thomson Ave, Cambridge CB3
0FF, UK

* The corresponding author for this article is Yan Yan Shery Huang.

Email: yysh2@cam.ac.uk

Section I - Tool Head Design

A controllable distance between the electrospinning syringe needle and support structure surface is crucial to facilitating the LEP process. The ability to calibrate the distance between the tip of any given nozzle, in this case the electrospinning syringe, and the build platform was an instrumental part of the printer's firmware customization. This allows flexibility in the length syringe tip used so printing can take place upon the grounded build plate, a glass slide or other elevated surfaces. Regular disassembly and reassembly of the electrospinning tool-head is also necessary to install fresh solution with the correct working parameters and to avoid nozzle clogging. This design requirement, in addition to the necessity in this configuration to switch tool-heads for alternating between different printing processes introduces a lot of scope for tool-head offsets in between mounting the different tools. Such offsets may prevent prints from having the appropriate precision and repeatability to enable this process. To address this, robust syringe loading and tool-head fastening on the tool-mount is essential.

Our design **Figure S1(a)** used three ball-in-vee groove features, along with a supplementary cone feature and magnets to provide a fastening to the tool-mount. This provides a kinematic coupling that is statically determinate, constraining all 6 degrees of freedom **Figure S1(b)**. The picking up mechanism is magnetic and the drop-off mechanism utilises the shearing force against fitted slots in the docking stations. This design is shown to be able to accommodate a large degree of misalignment, allowing the tool-head change to function even when the tool-head has moved around in the tool dock. Inside the electrospinning tool-head (see **S1(c)**), a vee-groove was also used to provide two of the point contact forces, while a third force was provided by a grub screw. This creates a determinate arrangement in two dimensions (i.e. it constrains the 3 degrees of freedom in 2D), and the use of a second grub

screw constrains the other degrees of freedom to maintain the distance between the syringe tip and printing substrate.

The robustness of the tool-head design was evaluated with time-lapse imaging and image analysis as illustrated in **S2(a)**. Displacement of the electrospinning syringe needle from a reference object was measured in X, Y and Z to evaluate the design performance, as shown in **S2(b)** and summarized in **Table S1**. The largest deviation from the mean position was in the Y axis. Even when the syringe was reassembled, the mean deviation of the syringe tip in Z was 7.5 μm which is acceptable precision to ensure reliable LEP processing. Overall, the design enables a tolerance of up to 9 mm, should the tool heads be misaligned in the tool dock. This tolerance provides 3D LEP with adequate robustness and precision without the need for further manipulation or interfering offset calibration.

To create multiple layers of fibers, it is important to ensure that subsequent PLA deposition do not damage the fibers already deposited. The default thermoplastic nozzle on an Ultimaker 2 system has a flattened tip with an outer tip width of 2 mm. Our studies show that this FFF nozzle cut off the fibers at the edge of the PLA support during the deposition of a new PLA layer. To minimize this effect, a conical printing nozzle with a narrow cone angle of $\sim 45^\circ$ and an outer tip width of 1mm was used see **S2(c)**. Integrating this hardware, we investigate how the working parameters of 3D-LEP affect the fiber patterning quality.

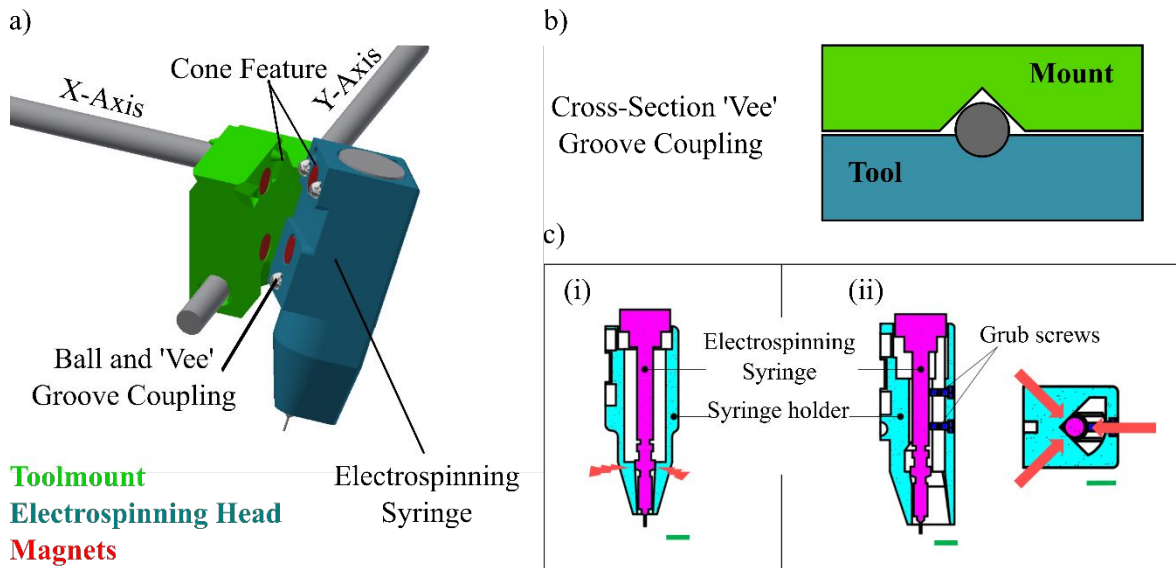


Figure S1. Design of the LEP tool head. a) Illustration of the LEP tool head; b) A cross-section of the kinematic coupling, which stabilizes the tool-head and provides robust alignment during a print. c) (i) shows the point of polymer charging and (ii) shows the features that constrain the syringe's degrees of freedom so that it is held at a secure distance from the build plate. Scale bars in c) represent 1 cm.

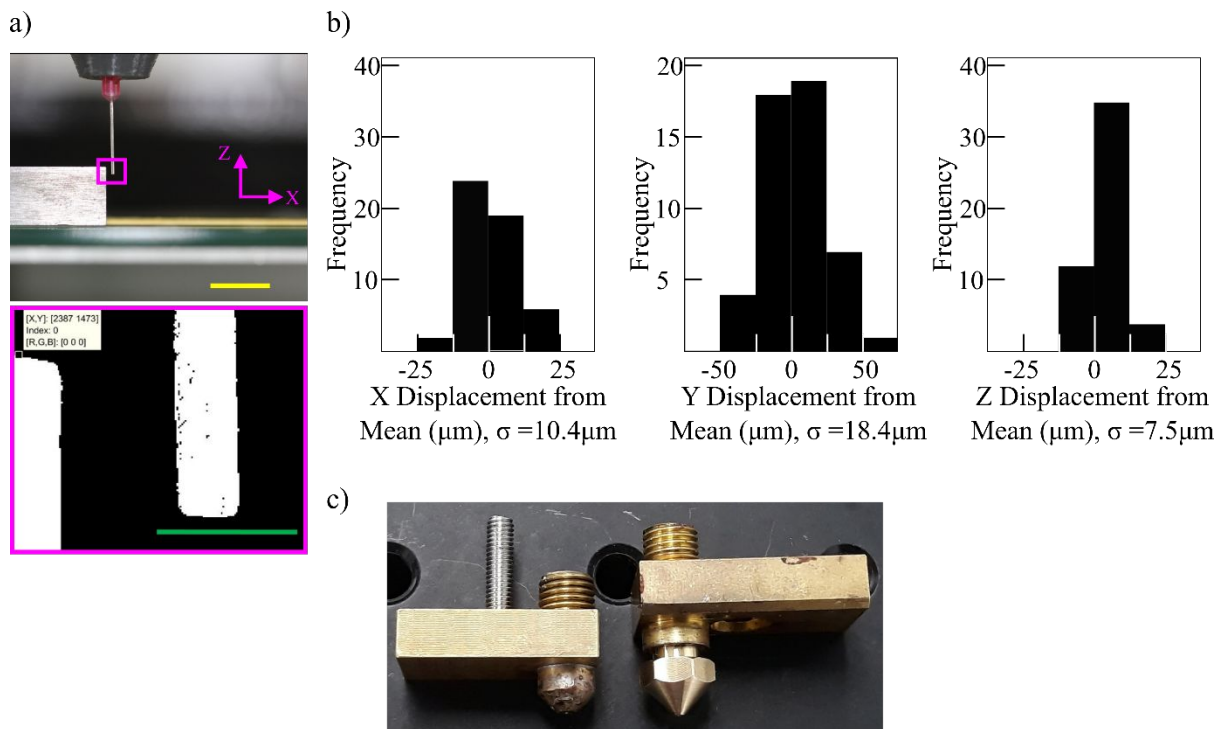


Figure S2. Assessment of Tool head Exchange Stability. a) Photographs and color threshold sequence depict the measurement procedure. Yellow scale bar represents 10 mm and green

scale bar represents 1 mm. b) Histograms show the XYZ displacement measurements collected after a sequence of tool switching sequences; c) Photo comparing the FFF nozzle geometry, left has a flattened tip whereas the right has a conical shape.

Table S1- Key data on tool head stability.

Misalignment	Displacement (mm)	9
Tolerance	Rotation (°)	17
Repeatability (µm)		12



Figure S3. Parametric characterization. Supporting images for support structure geometry parametric characterization, scale = 2 mm for photographs and 200 μm for top-down microscope images a) (ii) and c) (ii). A series of single layer suspended fiber arrays were created with different applied voltages for different support structure (a) pillar separation lengths; (b) heights and (c) different inter-fiber pitches. The suspension indicator (I_s) numbers are annotated on the pictures: yellow indicates the corresponding I_s values smaller than 1, with the prediction of suspended fibers; and red indicates the corresponding I_s values greater than 1, this predicts fibers falling out of suspension.

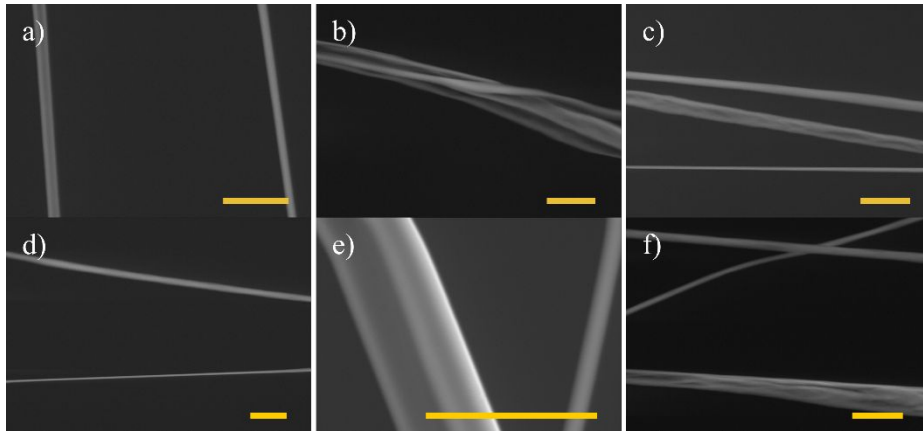
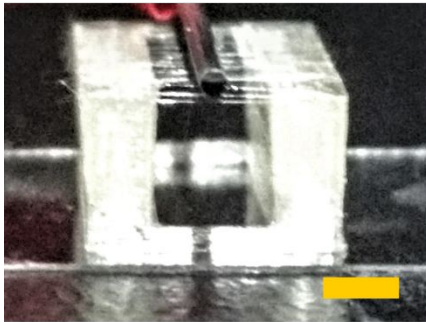


Figure S4. Scanning electron microscope images characterize the microstructure of suspended fibers showing fiber merging behavior. a-f) show ESEM images of different forms of microstructure, scale bars = 10 μm .

(a)



(b)

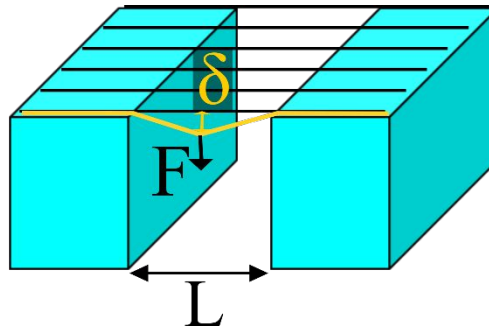


Figure S5. Mechanical characterization. (a) Shows a photograph of the point load coming into contact with a layer of fibers for mechanical testing, scale represents 2 mm. (b) Scheme illustrates the deflection measured with the loading applied on the fiber array.

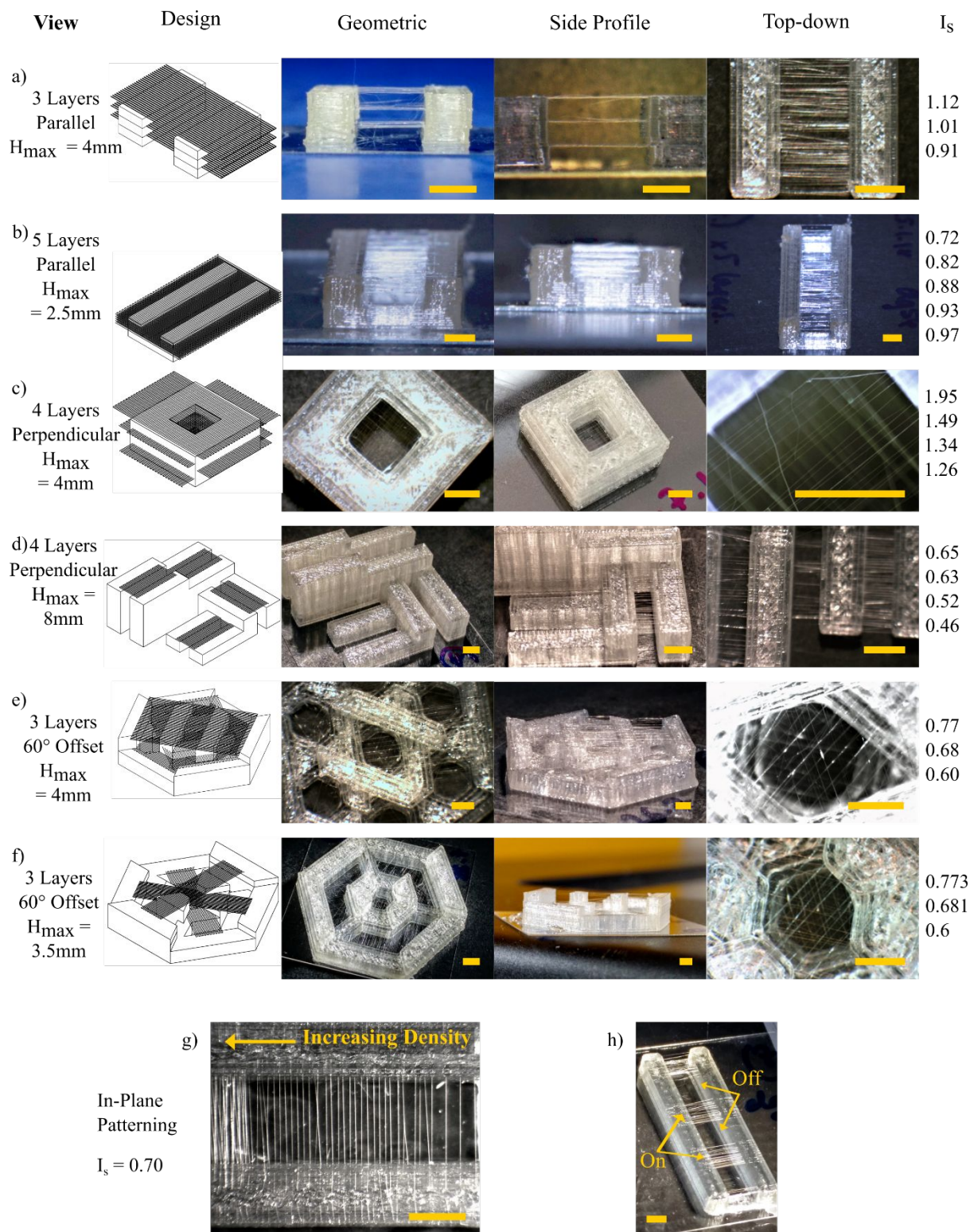


Figure S6 - Designable 3D layered fiber architectures. a) Three parallel layers of fibers with an inter-layer spacing of 1 mm; b) 5 layers with an inter-layer spacing of 300 μm ; c) Orthogonally layered fibers; d) Fiber layers suspended at different levels; e) and f) Multiple orientations of fibers in separate layers within a print. I_s numbers are in ascending order of

layers. g) A graded fiber density going along a layer of fibers; h) ‘On/off’ fiber patterning within a fiber plane. All scale bars represent 2 mm.

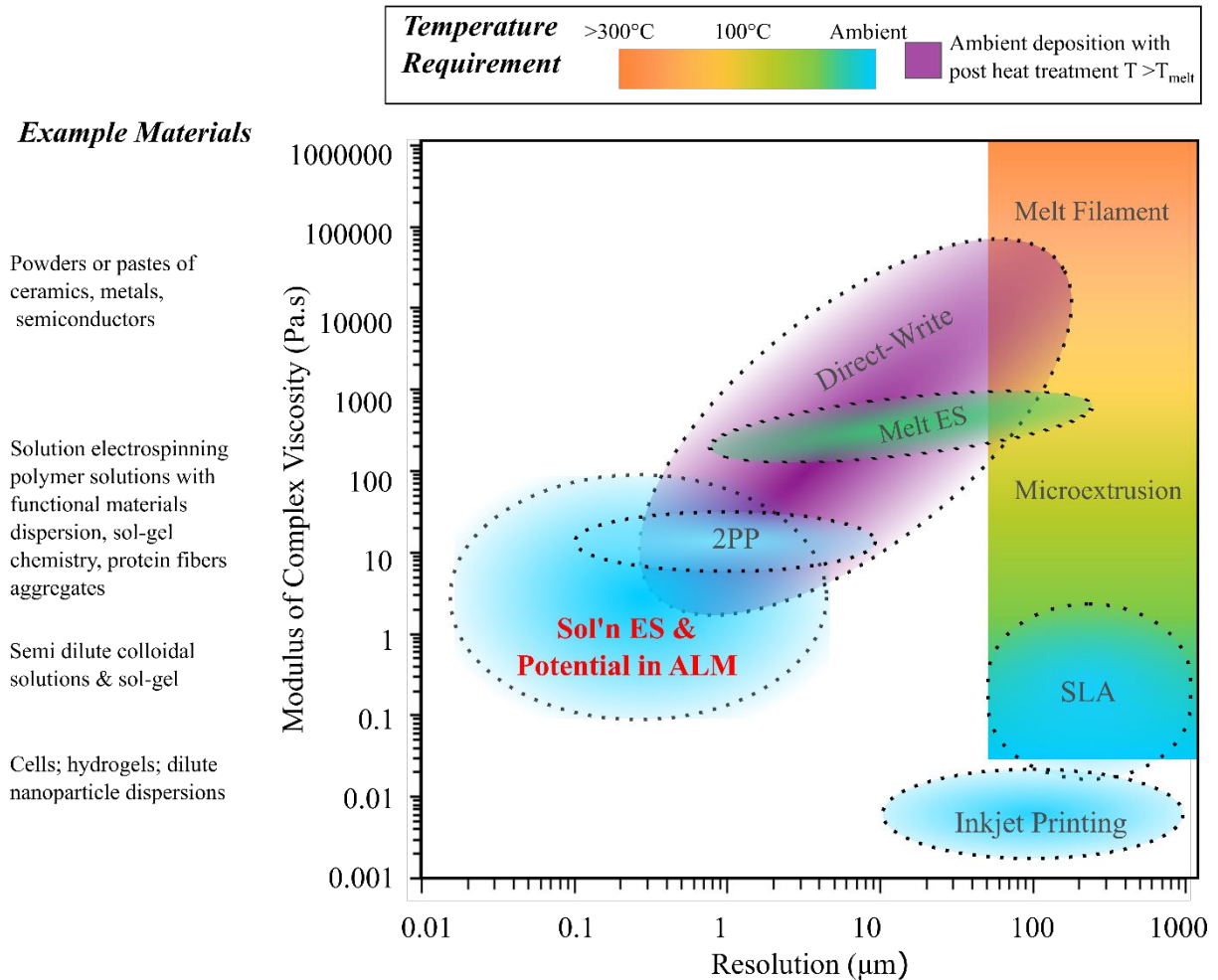


Figure S7. Map of feature resolution and modulus of complex viscoelasticity for selected 2.5 and 3D printing techniques, The modulus of complex viscosity is used as a generic indicator for the viscoelastic properties, which reflects the materials processing capability of a specific technique. References informing of this map are included in **Table S2**^{1,2,11–14,3–10}.

2PP = Two Photon- Polymerization; ALM= additive layer manufacture; ES =

Electrospinning or generic electrohydrodynamic fiber-based techniques; SLA=

Stereolithography. Based on previously published work¹⁵, reproduced under CC-BY license.

Copyright © 2018 The Author(s).

Table S2- Supporting references for Figure S7. To extract data from literature, we use the formula of modulus of complex viscosity $|\eta^*|$:

$$|\eta^*| = \sqrt{\eta'^2 + \eta''^2}$$

$$G^* = \omega \eta^*$$

$$|G^*| = \sqrt{G'^2 + G''^2}$$

Where ω is the rate at which the oscillatory rheometry is conducted, or the rate at which the “ink” is being extruded through the nozzle.

References	Technique	Resolution (μm)	Modulus of Complex Viscosity (Pa.s)
16,17	Extrusion incl. melt filament	100-1000+	0.03-1,000,000
18,19	Inkjet	10-1000+	0.002-0.020
20,21	SLA	50-1000+	0.021-1.77
22,23	2PP	0.1-10	5-25
11,12,24-26	Melt Electrospinning	0.8-21	120-1000
27-29	NFES	0.016-4	0.1-80.5
1-10	Direct-write	0.268-200	2-100,000

S8 Biological Experiments- Live/Dead Imaging and Immunostaining

A z-stack was acquired for the LIVE/DEAD study consisting of 10 slices over a depth of 285 μm using a 10x objective. Three-dimensional reconstruction of the fluorescent image slices was performed using Zeiss' proprietary software ZEN Lite. For the immunostaining, cells were fixed in 4% paraformaldehyde (PFA, Sigma-Aldrich) and permeabilized with 0.2% Triton 100X (Sigma-Aldrich) in phosphate buffered saline. Non-specific antibody interactions were blocked by incubating the cells with 4% albumin from bovine serum (BSA, Sigma-Aldrich, A7906) in PBS for 1 hr. For nuclear and cytoskeleton staining, CyTRAK (Sigma, 94403) and GFAP (Life Technologies, A12379) were used at 1:1000 dilutions in PBS. The devices were washed and then stored in PBS at 4 °C and fluorescence imaging was performed within 8 days from staining. Subsequently, fluorescent images were acquired by Leica SP5 confocal microscope using a 10x objective. A z-stack was captured over a depth of 151.16 μm with a 2.52 μm step size. Three-dimensional reconstruction of the confocal image slices was performed with Fiji ImageJ.

REFERENCES

- (1) Espinosa-Hoyos, D.; Jagielska, A.; Homan, K. A.; Du, H.; Busbee, T.; Anderson, D. G.; Fang, N. X.; Lewis, J. A.; Van Vliet, K. J. Engineered 3D-Printed Artificial Axons. *Sci. Rep.* **2018**, *8* (1), 478.
- (2) Hanson Shepherd, J. N.; Parker, S. T.; Shepherd, R. F.; Gillette, M. U.; Lewis, J. A.; Nuzzo, R. G. 3D Microperiodic Hydrogel Scaffolds for Robust Neuronal Cultures. *Adv. Funct. Mater.* **2011**, *21* (1), 47–54.
- (3) Barry, R. A.; Shepherd, R. F.; Hanson, J. N.; Nuzzo, R. G.; Wiltzius, P.; Lewis, J. A. Direct-Write Assembly of 3D Hydrogel Scaffolds for Guided Cell Growth. *Adv. Mater.* **2009**, *21* (23), 2407–2410.
- (4) Sun, K.; Wei, T.-S.; Ahn, B. Y.; Seo, J. Y.; Dillon, S. J.; Lewis, J. A. 3D Printing of Interdigitated Li-Ion Microbattery Architectures. *Adv. Mater.* **2013**, *25* (33), 4539–4543.
- (5) Ahn, J.-H.; Kim, H.-S.; Lee, K. J.; Jeon, S.; Kang, S. J.; Sun, Y.; Nuzzo, R. G.; Rogers, J. A.; Rogers, J. A.; Lewis, J. A. Heterogeneous Three-Dimensional Electronics by Use of Printed Semiconductor Nanomaterials. *Science* (80-.). **2006**, *314* (5806), 1754–1757.
- (6) Ahn, B. Y.; Lorang, D. J.; Duoss, E. B.; Lewis, J. A. Direct-Write Assembly of Microperiodic Planar and Spanning ITO Microelectrodes. *Chem. Commun.* **2010**, *46* (38), 7118.
- (7) Sun, L.; Parker, S. T.; Syoji, D.; Wang, X.; Lewis, J. A.; Kaplan, D. L. Direct-Write Assembly of 3D Silk/Hydroxyapatite Scaffolds for Bone Co-Cultures. *Adv. Healthc. Mater.* **2012**, *1* (6), 729–735.
- (8) Ghosh, S.; Parker, S. T.; Wang, X.; Kaplan, D. L.; Lewis, J. A. Direct-Write Assembly of Microperiodic Silk Fibroin Scaffolds for Tissue Engineering Applications. *Adv. Funct. Mater.* **2008**, *18* (13), 1883–1889.
- (9) Duoss, E. B.; Twardowski, M.; Lewis, J. A. Sol-Gel Inks for Direct-Write Assembly of Functional Oxides. *Adv. Mater.* **2007**, *19* (21), 3485–3489.
- (10) Gratson, G. M.; Xu, M.; Lewis, J. A. Microperiodic Structures: Direct Writing of Three-Dimensional Webs. *Nature* **2004**, *428* (6981), 386–386.
- (11) Wunner, F. M.; Wille, M.-L.; Noonan, T. G.; Bas, O.; Dalton, P. D.; De-Juan-Pardo, E. M.; Huttmacher, D. W. Melt Electrospinning Writing of Highly Ordered Large Volume Scaffold Architectures. *Adv. Mater.* **2018**, *30* (20), 1706570.
- (12) Hrynevich, A.; Elçi, B. Ş.; Haigh, J. N.; McMaster, R.; Youssef, A.; Blum, C.; Blunk, T.; Hochleitner, G.; Groll, J.; Dalton, P. D. Dimension-Based Design of Melt Electrowritten Scaffolds. *Small* **2018**, *14* (22), 1800232.
- (13) Coppola, S.; Vespini, V.; Nasti, G.; Gennari, O.; Grilli, S.; Ventre, M.; Iannone, M.; Netti, P. A.; Ferraro, P. Tethered Pyro-Electrohydrodynamic Spinning for Patterning Well-Ordered Structures at Micro- and Nanoscale. *Chem. Mater.* **2014**, *26* (11), 3357–3360.
- (14) Coppola, S.; Nasti, G.; Todino, M.; Olivieri, F.; Vespini, V.; Ferraro, P. Direct Writing of Microfluidic Footpaths by Pyro-EHD Printing. *ACS Appl. Mater. Interfaces* **2017**, *9* (19), 16488–16494.
- (15) Gill, E. L.; Li, X.; Birch, M. A.; Huang, Y. Y. S. Multi-Length Scale Bioprinting towards Simulating Microenvironmental Cues. *Bio-Design Manuf.* **2018**, *1* (2), 77–88.
- (16) Murphy, S. V.; Atala, A. 3D Bioprinting of Tissues and Organs. *Nat. Biotechnol.* **2014**, *32* (8), 733–785.
- (17) Smay, J. E.; Nadkarni, S. S.; Xu, J. Direct Writing of Dielectric Ceramics and Base Metal

- Electrodes. *Int. J. Appl. Ceram. Technol.* **2007**, *4* (1), 47–52.
- (18) Derby, B. Inkjet Printing of Functional and Structural Materials: Fluid Property Requirements, Feature Stability, and Resolution. *Annu. Rev. Mater. Res.* **2010**, *40* (1), 395–414.
- (19) Truby, R. L.; Lewis, J. A. Printing Soft Matter in Three Dimensions. *Nature* **2016**.
- (20) Tumbleston, J. R.; Shirvanyants, D.; Ermoshkin, N.; Januszewicz, R.; Johnson, A. R.; Kelly, D.; Chen, K.; Pinschmidt, R.; Rolland, J. P.; Ermoshkin, A.; Samulski, E. T.; DeSimone, J. M. Continuous Liquid Interface Production of 3D Objects. *Science (80-.)*. **2015**, *347* (6228), 1349–1352.
- (21) Stampfl, J.; Baudis, S.; Heller, C.; Liska, R.; Neumeister, A.; Kling, R.; Ostendorf, A.; Spitzbart, M. Photopolymers with Tunable Mechanical Properties Processed by Laser-Based High-Resolution Stereolithography. *J. Micromechanics Microengineering* **2008**, *18* (12), 125014.
- (22) Zhou, X.; Hou, Y.; Lin, J. A Review on the Processing Accuracy of Two-Photon Polymerization. *Cit. AIP Adv.* **2015**, *5*, 030701.
- (23) Sun, H.-B.; Kawata, S. Two-Photon Photopolymerization and 3D Lithographic Microfabrication; Springer, Berlin, Heidelberg, 2006; pp 169–273.
- (24) Brown, T. D.; Dalton, P. D.; Hutmacher, D. W. Direct Writing By Way of Melt Electrospinning. *Adv. Mater.* **2011**, *23* (47), 5651–5657.
- (25) Hochleitner, G.; Jüngst, T.; Brown, T. D.; Hahn, K.; Moseke, C.; Jakob, F.; Dalton, P. D.; Groll, J. Additive Manufacturing of Scaffolds with Sub-Micron Filaments via Melt Electrospinning Writing. *Biofabrication* **2015**, *7* (3), 035002.
- (26) Mota, C.; Puppi, D.; Gazzarri, M.; Bártolo, P.; Chiellini, F. Melt Electrospinning Writing of Three-Dimensional Star Poly(ϵ -Caprolactone) Scaffolds. *Polym. Int.* **2013**, *62* (6), 893–900.
- (27) Bisht, G. S.; Canton, G.; Mirsepassi, A.; Kulinsky, L.; Oh, S.; Dunn-Rankin, D.; Madou, M. J. Controlled Continuous Patterning of Polymeric Nanofibers on Three-Dimensional Substrates Using Low-Voltage Near-Field Electrospinning. *Nano Lett.* **2011**, *11* (4), 1831–1837.
- (28) Xue, N.; Li, X.; Bertulli, C.; Li, Z.; Patharagulpong, A.; Sadok, A.; Huang, Y. Y. S. Rapid Patterning of 1-D Collagenous Topography as an ECM Protein Fibril Platform for Image Cytometry. *PLoS One* **2014**, *9* (4), e93590.
- (29) Zheng, G.; Li, W.; Wang, X.; Wu, D.; Sun, D.; Lin, L. Precision Deposition of a Nanofibre by Near-Field Electrospinning. *J. Phys. D. Appl. Phys.* **2010**, *43*, 415501.